AGU PUBLICATIONS

JGR

Journal of Geophysical Research: Atmospheres

RESEARCH ARTICLE
10.1002/2016JD025910

Key Points:
- Satellite- and ground-based data sets used to delineate the diurnal tide variability at low latitudes
- Certain peculiarities in long-term tidal variability as observed in radar winds not seen in satellite data
- Solar influence on densities suggested to be causing the solar cycle signature of tides observed from ground

Correspondence to:
S. Gurubaran,
gurubara@iigs.iigm.res.in

Citation:
Singh, D., and S. Gurubaran (2017), Variability of diurnal tide in the MLT region over Tirunelveli (8.7°N), India: Consistency between ground- and space-based observations, *J. Geophys. Res. Atmos.*, *122*, 2696–2713, doi:10.1002/2016JD025910.

Received 11 SEP 2016
Accepted 20 FEB 2017
Accepted article online 22 FEB 2017
Published online 7 MAR 2017

Variability of diurnal tide in the MLT region over Tirunelveli (8.7°N), India: Consistency between ground- and space-based observations

Dupinder Singh[1] and **S. Gurubaran**[1]

[1]Indian Institute of Geomagnetism, Navi Mumbai, India

Abstract Atmospheric tides propagating upward into the mesosphere-lower thermosphere region carry the variability from the lower atmosphere and influence the energy and momentum budgets of this region and above. A comprehensive understanding of these variabilities thus becomes important. In this work, we study the seasonal and interannual variabilities of the diurnal tides, in particular, the migrating DW1 (westward, wave number 1) tide and the nonmigrating DE3 (eastward, wave number 3) tide from two different platforms. Long-term observations from the MF radar at Tirunelveli (8.7°N, 77.8°E) constitute one data set. Temperature and wind data from Sounding of the Atmosphere using Broadband Emission Radiometry and TIMED Doppler Interferometer observations from the TIMED satellite mission constitute the other. Continuous radar observations yield long data records with high temporal resolution. Space-based observations, on the other hand, are relatively short but provide spatiotemporal information, the latter being useful in separating migrating and nonmigrating components. In this work, the consistency between the tidal signatures obtained from the ground- and space-based platforms is examined and subtle differences between the two data sets are brought out. One particular feature pertains to a possible solar cycle influence on the diurnal tide, a feature which is more prominently seen in radar observations, though restricted to a certain epoch of the solar cycle. A solar cycle dependence of the zonal mean densities observed in satellite data sets at similar altitudes appears to be a plausible source for the observed solar cycle signature in the diurnal tide, although the role of other agencies in modulating the diurnal tide activity in the solar cycle time periods cannot be ruled out.

1. Introduction

Tides are the most prominent features in the mesosphere-lower thermosphere (MLT) region. These are global-scale oscillations in various atmospheric parameters such as temperature, wind, neutral density, and pressure. These oscillations have time periods which are integral fractions of the length of a solar or a lunar day. While most work was focused on diurnal (24 h) and semidiurnal (12 h) tides, and their sources are reasonably well understood, higher-frequency tides have also been observed. Nonlinear interaction between diurnal, semidiurnal, and terdiurnal tides are known to generate tides of higher frequency.

Atmospheric tides can be generated thermally (solar tides) and gravitationally (lunar tides), with thermally generated tides having much larger amplitude than the gravitational tides. Solar tides can be broadly classified into migrating and nonmigrating tides. Migrating tides are generated by solar heating and follow the apparent motion of the Sun. Major sources of migrating tides are the absorption of IR radiation by water vapor in the troposphere and the UV radiation by ozone in the stratosphere. Migrating tides can also be generated in the thermosphere through absorption of UV/EUV radiation by oxygen atoms and molecules [*Forbes*, 1995]. Nonmigrating tides are generated by longitudinally varying sources, for example, the longitudinally varying tropospheric latent heat release due to land-sea contrast and sea surface temperatures [*Hagan and Forbes*, 2002, 2003]. Nonlinear interaction between migrating tides and stationary planetary waves is also known to be a source of nonmigrating tides [*Hagan and Roble*, 2001; *Mayr et al.*, 2005].

Tides excited in the lower atmosphere propagate to the upper atmosphere with amplitudes exponentially increasing with altitude. Within the MLT region, with their large amplitudes, tides can lead to much larger variation in winds, temperature, density, and many other parameters, thus dominating the meteorology of the MLT region (80–160 km) [*Forbes et al.*, 2008]. Most of the tides carrying their energy and momentum upward attain their largest amplitudes between 100 and 120 km before they undergo damping due to molecular diffusion. At these altitudes, they deposit the energy and momentum they carry from the lower

atmosphere. With their large vertical wavelengths, tides thus provide an efficient mechanism for the vertical coupling of the atmosphere. Further, some of the vertically propagating tides communicate the variability of the lower and middle atmosphere to the upper atmosphere.

Tides are characterized by their latitudinal structure, longitudinal wave number, and periodicity. It has been appreciated for a while that ground-based observations from one or a few sites cannot fully resolve the latitudinal and longitudinal structure, although they have high temporal resolution, whereas satellites can provide spatiotemporal information, but with limited temporal resolution. Further, radars have been in use over a few decades at a number of sites across the globe thus offering relatively longer data sets.

As can be expected, any comparison of the MLT tidal signatures between the two data sets poses several complexities. This is due to the different nature of the two observations, as the sampling volumes probed by the two techniques are considerably different [*Hasebe et al*., 1997]. Ground-based observations may detect many features that are of local nature (pseudo-tides, for example). It has been previously suggested that most of the issues between the two data sets have been resolved to a large extent [*Ward et al*., 2010], but, as we will see in the present work, considerable discrepancies between the two still exist, especially, when longer duration data sets are used.

One typical limitation of single-station ground-based-observations is their inability to distinguish nonmigrating components from the migrating tides. As noted above, ground-based observations provide only the temporal information and no spatial information. For example, the zonal wave number of a given tide cannot be ascertained from single-site observations. What is observed on the ground is, in fact, a superposition of all tidal components, migrating and nonmigrating included, having the same periodicity but different spatial structures (zonal wave number). Such a drawback of ground-based observations limits their usability in investigating long-term variabilities of various tidal components, as the sources of variability could be different for migrating and nonmigrating tides.

Advent of satellite-based techniques had facilitated the diagnostics of tidal signatures observed by ground-based instruments. A precessing satellite, for example, can observe and resolve both nonsynchronized (nonmigrating) and synchronized (migrating) tides over a given time window. The spatiotemporal nature of satellite-based observations thus allows us to delineate migrating and nonmigrating components.

A systematic and an extensive comparison between these two types of observations was carried out during the Climate And Weather of Sun-Earth System (CAWSES) program [*Ward et al*., 2010], albeit for a limited period, wherein tidal signatures sampled by ground-based observations were compared with those derived from a superposition of various tidal components retrieved from the satellite observations. There have been few other such reports as well [*Kishore Kumar et al*., 2014; *John et al*., 2011; *Hasebe et al*., 1997]. However, no study has been carried out to examine the agreement or disagreement between the two sets of tidal observations in longer time scales.

Previously, there have been a few studies showing the disagreement between the tidal signatures derived from ground stations at different longitudes [e.g., *Gurubaran et al*., 2009]. In this context, it was suggested that most of the longitudinal variability arises because of the nonmigrating tidal components and changes in the background atmosphere [*Chang et al*., 2012]. Certain other differences have been attributed to window sizes [*Kishore Kumar et al*., 2014] used for extracting tides and individual vertical resolution of the instruments [*Ward et al*., 2010].

In this paper, we analyze the diurnal tide signatures observed by a ground-based station and the differences that show up when these observations are compared with tidal fields derived from the satellite observations. For this purpose, we have used the data obtained by the MF radar operating from Tirunelveli (8.7°N, 77.8°E), India, for the period of 1993–2011. For delineating global tides, we use observations obtained from the Sounding of the Atmosphere using Broadband Emission Radiometry (SABER) and TIMED Doppler Interferometer (TIDI) instruments on board the Thermosphere Ionosphere Mesosphere Energetics and Dynamics (TIMED) satellite as described in section 2. The wave number spectra for the diurnal temperatures and winds from SABER and TIDI instruments are presented in section 3. The focus in section 4 is on delineating the seasonal and long-term climatology of DW1 and DE3 tides in temperatures and winds. In section 5 we present an interesting finding linking the long-term variability of diurnal tide in radar observations with the satellite derived zonal mean density fields. Smaller densities during solar minimum years of 2007, 2008,

and 2009 when the tides were stronger and larger densities during the solar maximum years of 1999, 2000, and 2001 when the tides were weaker imply a solar cycle influence on tidal winds. In section 6, we reconstruct the tidal fields from SABER/TIDI observations for the low-latitude ground-based radar site, Tirunelveli. Individual tidal signatures thus obtained are then compared with the radar observations over selected altitudes. Although there is an overall agreement between the tidal signatures obtained from the two data sets, the differences are significant, especially in the zonal wind. In section 7 we present a discussion of the results in the context of our current understanding of dominant migrating and nonmigrating tides at low latitudes. We focus on certain peculiarities of the observed features that were not reported earlier.

2. Data and Methodology

Three different data sets have been used in this study, namely, the hourly wind data from the MF radar, the temperature measurements from SABER, and the neutral wind measurements from TIDI. The MF radar at Tirunelveli has been operating since 1993 (see *Rajaram and Gurubaran* [1998] for experimental details and the analysis procedure adopted for the determination of winds). The observed data for the zonal and meridional winds are averaged into hourly values. There are a few major gaps in the radar data during 2009 and 2010, as the radar was not operational then.

For temperatures, SABER v2.0 data from http://saber.gats-inc.com/data.php are used. Version 2.0 includes many improvements over the previous version 1.7, as mentioned at http://saber.gats-inc.com/data_v2.php. SABER is a 10-channel radiometer scanning the atmosphere from 1.27 μm to 17 μm. SABER measurements extend over 20–120 km in altitude and 82°N–53°S (alternate hemispheres coverage with yaw cycle) in latitude. The present analysis is restricted to 40°N to 40°S latitude because of the uneven coverage at high latitudes. Data validations and relative errors can be found in *Garcia- Comas et al*. [2008] and *Riggin and Lieberman* [2013]. The errors in temperature are ~3 K or less below 105 km. The present analysis is restricted to 105 km as uncertainties are much larger for higher altitudes.

For global winds, TIDI level 3 vector winds are used, which can be accessed at ftp://tidi.engin.umich.edu/tidi/vector/. TIDI is a limb-scanning Fabry-Perot interferometer and is used to observe the emissions from OI (557.7 nm, 630.0 nm, and 844.6 nm), OII (732 nm), O2 (762 nm and 861 nm), Na (589 nm), and OH (550 nm–900 nm) lines yielding measurements of Doppler winds and temperature. TIDI initially had performance issues because of ice deposition on telescopes and light leakage [*Skinner et al*., 2003]. These issues were resolved to a great extent following two roll maneuvers of the spacecraft in 2003 and gradual sublimation of ice over time. There has been considerable improvement in the data quality since then. Further, it may be noted that we use TIDI data of Version 11, which was the outcome of an improved background removal model utilized to minimize any further effect of light leak. The TIDI data validation was discussed in *Killeen et al*. [2006]. The performance summary of the TIDI instrument can be found at http://tidi.engin.umich.edu/whats_new/20040521_02/Scattering_trend_files/v3_document.htm.

The present study utilizes the SABER data for the period of 2002–2011, TIDI data for the period of 2004–2011, and radar data for the period of 1993–2011. Least squares fitting is used to retrieve tidal signatures from these data sets. With a precession of 3% per day, TIMED takes ~60 days to sample all local times with measurements from both ascending and descending orbits. The window size used in this study is thus 60 days. For comparative study, the same window size is used while analyzing the radar data.

While deriving tidal signatures from the radar data, least squares fits are applied to the 2 month composite means. This is done only for windows for which the composite mean has at least 18 out of 24 h available, and each hour has a contribution from at least 10 days out of 60 days. Similarly, least squares fits are applied to SABER temperatures and TIDI winds for each 2 month window. The following equation is used to fit the satellite data (temperatures/winds) for a given 2 month window [*Pancheva and Mukhtarov*, 2011].

$$\Theta(t,\lambda) = \Theta_0 + \Theta_r t + \sum_{j=1}^{4}\sum_{s=-3}^{3} A_{j,s}\cos\left[\frac{2\pi}{24T_j}t - \frac{2\pi}{360}s\lambda - \frac{2\pi}{360}\varphi_{j,s}\right] + \sum_{s=1}^{3} B_s\cos\left[\frac{2\pi}{360}s\lambda - \frac{2\pi}{360}\psi_s\right] + \sum_{k=1}^{2}\sum_{s=-4}^{4} C_{k,s}\cos\left[k\frac{2\pi}{24}t - \frac{2\pi}{360}s\lambda - \frac{2\pi}{360}\gamma_{k,s}\right] + R(t,\lambda) \quad (1)$$

In the above equation, t is time (in UT hours) and λ is longitude in degrees. This equation includes traveling and stationary planetary waves. The first and second terms account for the mean temperatures/winds and temperature/wind trends, respectively. Trends (appearing in the second term) due to longer period oscillations like the semiannual oscillation (SAO), which is so prominent at low latitudes, can have an effect on the estimates of tidal amplitudes, if not properly taken into account. The third, fourth, and fifth terms represent traveling planetary waves, stationary planetary waves, and tides, respectively. The two indices on the double summation correspond to the time period and zonal wave number, respectively. In the above, $T_j = 24$, 17, 11, and 5.5 are planetary wave periods in days. As noted in *Pancheva and Mukhtarov* [2011], planetary waves are well known to have periods near 5, 10, and 16 days. The spectral analysis performed by these authors indicated the dominant periods to show up at 5.5 days, 11 days, and 17 days, respectively. Further, the 24 day wave has been reported to be a regular feature observed in the stratosphere and mesosphere [*Pancheva and Mukhtarov*, 2011 and references therein].

In the above equation, s is the zonal wave number; negative (positive) wave number represents westward (eastward) propagating waves. R is the residual emerging from the fitting process. The fifth term represents tides and includes both semidiurnal and diurnal migrating and nonmigrating components up to wave number 4 (both eastward and westward). The migrating and nonmigrating tides and stationary and traveling planetary waves are all simultaneously fit to the data to avoid any aliasing.

The above equation is converted into a linear form and then solved as a system of linear equations. The satellite data are divided into 10° latitude bins and 5 km altitude bins. For each bin and 60 day window, all available (t,λ) pairs are extracted and fed to the above equation. We accept the fitted results only if there are at least 500 such pairs for a given window and bin. Any data point greater than 3σ is considered as an outlier and is removed. This window is then moved by 1 day, and the whole data period is then covered. The same procedure is applied for analyzing the radar data, but here the fit equation is a function of time only. We start with an initial 2 month window and take the composite mean for each hour. Then, a least squares fit is applied to this hourly data. This fit includes the diurnal, semidiurnal, and terdiurnal components. The window is then moved by 1 day to obtain the daily signatures. Any window with significant data gaps is skipped so as to avoid spurious results. The daily signatures retrieved are averaged for each month.

The tides extracted from the satellite observations are reconstructed for the location of the ground station, Tirunelveli. We use the following expressions for the reconstruction:

$$a = \sum_i \left[C_i * \cos\left(\frac{2\pi s_i \lambda}{360}\right) - S_i * \sin\left(\frac{2\pi s_i \lambda}{360}\right) \right] \tag{2}$$

$$b = \sum_i \left[C_i * \sin\left(\frac{2\pi s_i \lambda}{360}\right) + S_i * \cos\left(\frac{2\pi s_i \lambda}{360}\right) \right] \tag{3}$$

where C_i and S_i are the coefficients of the cosine and sine terms of the linearized equations, respectively; s_i is the zonal wave number; and λ is the longitude of the ground station. The amplitude, A, and phase, φ, of the wave component to be deduced are calculated by using the above coefficients:

$$A = \sqrt{a^2 + b^2} \tag{4}$$

$$\varphi = \frac{360}{2\pi} \tan^{-1}\left(\frac{b}{a}\right) \tag{5}$$

3. Wave Number Spectra of the Diurnal Tide Over the 0–10° Latitude Grid

To examine the relative dominance of tidal components, the estimated amplitudes for various wave numbers (eastward and westward) are plotted on a wave number versus time (in terms of month) graph for the two altitudes, 87.5 km and 97.5 km. The spectra include both migrating and nonmigrating components up to wave number 4. This allows for selection of the dominant tidal components for reconstruction at chosen altitudes.

Figure 1a shows the wave number spectrum of the diurnal tide in temperature over the equator at an altitude of 87.5 km, as derived from SABER. It can be seen that DW1 (westward migrating component with wave number 1) is the major diurnal component at this altitude along with DE3 (eastward nonmigrating component

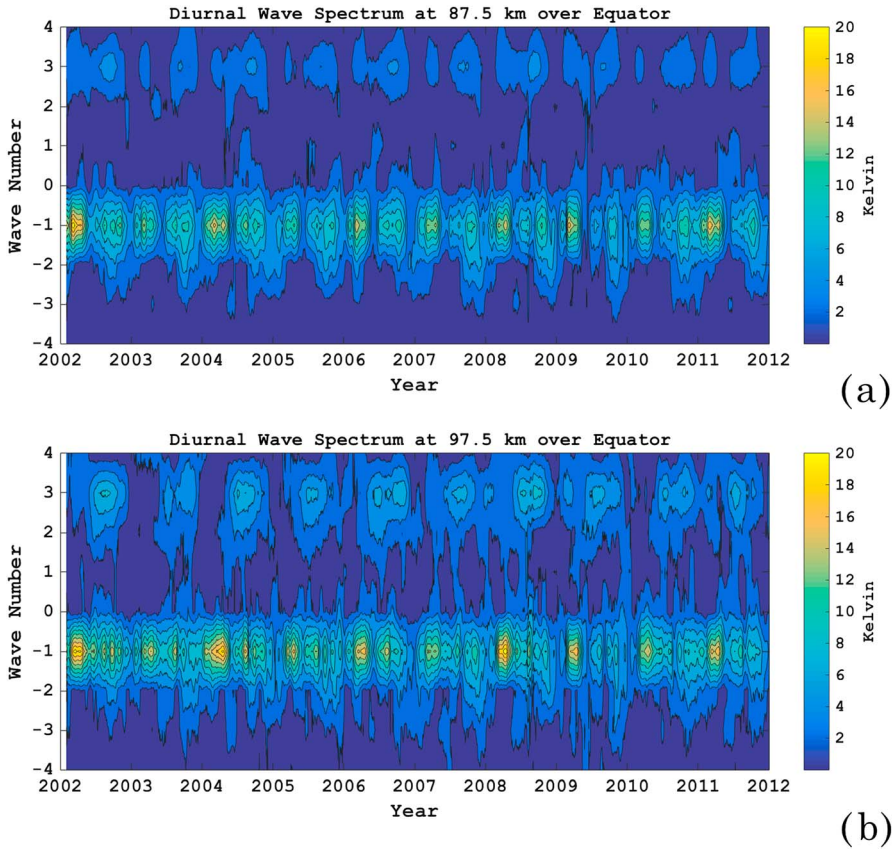

Figure 1. (a) Diurnal wave number spectrum for SABER temperatures at 87.5 km over equator. (b) Same as Figure 1a but for the height of 97.5 km.

with wave number 3) tide, which has relatively smaller amplitudes. DW1 attains a maximum amplitude of more than 18 K, whereas DE3 amplitudes are less than 6 K. DW2 (westward nonmigrating component with wave number 2) reveals amplitudes of the same order as those of DE3. These three waves should suffice for the reconstruction of the resultant diurnal component at this altitude. There is a noticeable quasi-biennial oscillation (QBO)-type variation in both DW1 and DE3, which will be discussed later.

The diurnal wave number spectrum at higher altitudes includes notable contribution from nonmigrating components. Figure 1b shows the wave number spectrum for the diurnal temperature over the equator at an altitude of 97.5 km. Contribution of DE3 is larger (~8–9 k) at this altitude when compared to that at 87.5 km, whereas DW2 reveals similar amplitudes as at 87.5, although DW1 is still the dominant tidal component even at 97.5 km. As reported earlier, DE3 maximizes at 110 km with a peak amplitude of ~13 K (not shown here) [e.g., *Truskowski et al.*, 2014], whereas DW2 attains a maximum amplitude of ~5 K. Migrating DW1 component can have amplitudes as large as ~20 K, especially during the eastward phase of the QBO. The contributions from other nonmigrating components, namely, D0 (stationary tide), DE1 (eastward nonmigrating tide with wave number 1), and DE2 (eastward nonmigrating tide with wave number 2), can also be noticed at higher altitudes, but with much smaller amplitudes (in the range of 1–3 K). There is a persistent QBO-like feature seen in the dominant tidal components up to 2008, and thereafter, it seems to have been shifted in phase. As we will see later in section 5, this feature is consistent with radar observations.

The wave number spectra of the diurnal winds as derived from TIDI shown in Figures 2a–2d are rather interesting, as they reveal the dominance of tides appearing differently in the zonal and meridional wind components. The meridional component has little but intermittent contribution from the nonmigrating tides. At 87.5 km, the diurnal tide in the meridional component is dominated by DW1 (Figure 2a). It reaches a maximum amplitude of more than 25 m s^{-1}, whereas other diurnal tide components have amplitudes of up to ~7 m s^{-1}, but their occurrences are highly intermittent. At 97.5 km, the contribution from the eastward

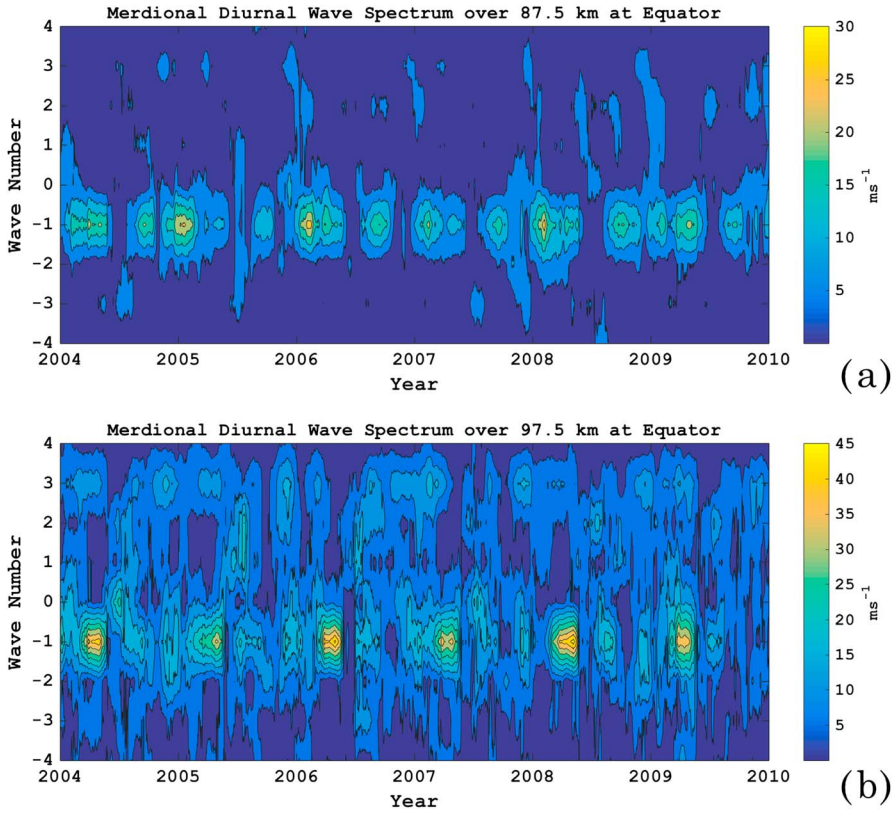

Figure 2. (a) Diurnal wave number spectrum for the meridional wind at 87.5 km over equator obtained from TIDI observations. (b) Same as Figure 2a but for the height of 97.5 km.(c) Diurnal wave number spectrum for the zonal wind at 87.5 km over equator obtained from TIDI observations. (d) Same as Figure 2c but for the height of 97.5 km.

propagating nonmigrating tides is significant, with DE3 showing amplitudes in excess of 30 m s^{-1} (Figure 2d). It may be noted that the first symmetric mode of DE3 tide has been recognized to be a diurnal Kelvin wave with larger amplitudes in zonal wind [*Forbes et al*., 2003a]. Apart from DE3, the zonal standing waves (wave number zero) also show notable contribution. The DW1 tide continues to dominate at higher altitudes with amplitudes exceeding 40 m s^{-1}. Westward propagating nonmigrating tides are relatively smaller in amplitudes in this altitude region. There is a consistent QBO-like feature noticed in the diurnal tide in the meridional component at 97.5 km (Figure 2b).

A significant feature to take note of in Figure 2 is that in contrast to the meridional component, the zonal component shows noticeable contribution from the nonmigrating tides even at 87.5 km (Figure 2c) and their competing presence at 97.5 km (Figure 2d). At 87.5 km, the amplitude of DE3 is almost half that of DW1, whereas at 97.5 km DE3 reveals larger amplitudes on many occasions. Further, the DE3 tide seems to exhibit QBO-like behavior.

Also to be taken note of is the seasonal behavior of DW1 in the zonal component. Apart from the equinoctial maxima in DW1 amplitudes, which is a known feature, there is an additional peak appearing during June–July (see Figure 2c). *Gurubaran and Rajaram* [1999] first reported this additional peak in the zonal component from the MF radar observations at Tirunelveli.

4. Seasonal and Long-Term Climatology of DW1 and DE3 in Temperatures and Winds

In this section, we delineate the climatology of DW1 at 87.5 km and DE3 at 97.5 km as derived from SABER (2002–2013) and TIDI (2004–2013) observations. In recent years several studies based on SABER observations have presented the climatologies of diurnal tide in seasonal time scales [e.g., *Zhang et al*., 2006; *Oberheide*

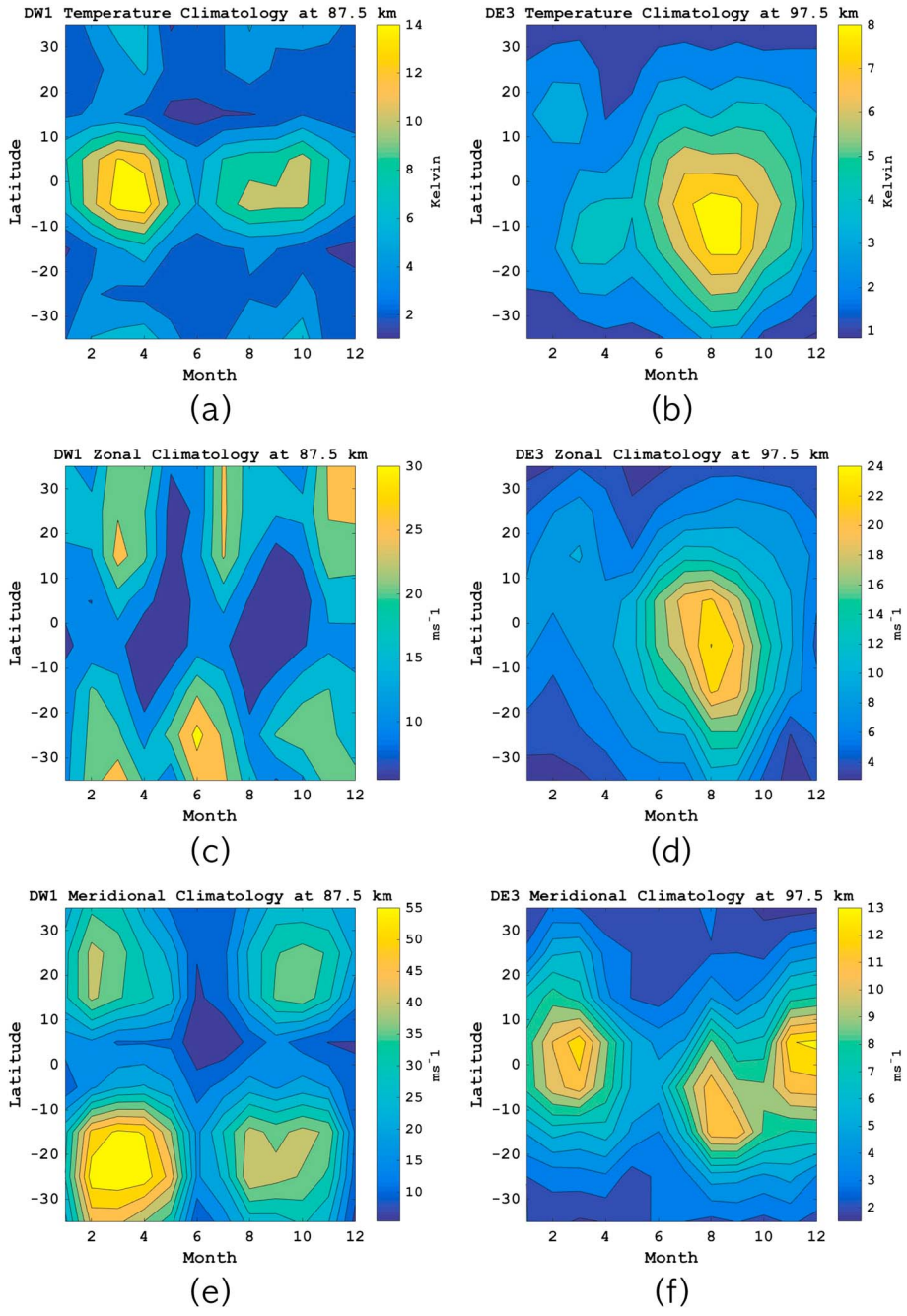

Figure 3. (a) The climatological amplitude of DW1 obtained from SABER temperature observations at 87.5 km. (b) Same as Figure 3a but for DE3 climatological amplitude at 97.5 km. (c) The climatological amplitude of DW1 in zonal wind at 87.5 km from TIDI observations. (d) Same as Figure 3c but for DE3 climatological amplitude at 97.5 km. (e) The climatological amplitude of DW1 in meridional wind at 87.5 km from TIDI observations. (f) Same as Figure 3e but for DE3 climatological amplitude at 97.5 km.

et al., 2006; *Mukhtarov et al*., 2009; *Sakazaki et al*., 2012; *Gan et al*., 2014]. Here we present similar results from SABER and also include results from TIDI observations to compare the seasonal variation of tidal components from two different data sets.

It has been recognized that the seasonal and latitudinal behavior of tides is different in different parameters. Hough modes can be used to derive the latitudinal structure of given tide in various parameters. Here we

use actual observations to investigate the relation between DW1 and DE3 in temperature and wind in terms of their seasonal variations. Climatological amplitudes derived from SABER and TIDI are used here. The consistency of DE3 tides as observed by SABER and TIDI has been demonstrated earlier [*Oberheide and Forbes*, 2008].

From here onward, the DW1 in temperature (*T*), zonal wind (*U*), and meridional wind (*V*) will be represented by DW1(*T*), DW1(*U*), and DW1(*V*), respectively. A similar notation is used for nonmigrating components. For the radar observations, the diurnal tide components corresponding to meridional and zonal winds will be denoted by RDm and RDz, respectively, where m and z refer to meridional and zonal components, respectively. D(*x*) denotes the reconstructed diurnal tide for the given location in parameter *x* (*x* can be *U*, *V*, or *T*).

It is very often noticed that the DW1 tide shows similar intraannual variability in *T* and *V*. However, their latitudinal structure is different, with DW1(*T*) maximizing at equator and DW1(*V*) maximizing in the tropics (see Figures 3a and 3e). Both DW1(*T*) and DW1(*V*) show an SAO-like behavior with maximum amplitudes detected during equinoxes. Further, at 87.5 km, the amplitudes of DW1(*V*) (Figure 3e) are twice those of DW1(*U*) (Figure 3c), although this difference does not seem to persist over the equator. The climatologies of DW1(*U*), DW1(*V*), and DW1(*T*) from UARS were reported earlier by *Svoboda et al*. [2005]. In their results, DW1(*V*) showed triannual variability in the Northern Hemisphere, but TIDI-derived DW1(*V*) climatology was predominantly semiannual in both hemispheres. Similar discrepancy for DW1(*U*) was also noticed.

It is evident in Figures 3b and 3d that both DE3(*T*) and DE3(*U*) at 97.5 km show dominantly an annual oscillation with maxima during August month. It may be noted that the amplitudes of DE3(*U*) are twice those of DE3(*V*) (shown in Figure 3f), thus indicating the dominance of DE3 in the zonal wind at the equator. This is expected as DE3 is known to be a diurnal Kelvin wave with a larger amplitude in zonal wind [*Forbes et al*., 2003a].

We conclude from the above that the DW1 tidal response is stronger in meridional wind, whereas the DE3 tidal response is stronger in the zonal wind, although their relative contribution to the given wind component changes with altitude, latitude, and season. It may be noted that DW1 is stronger at 87.5 km, whereas DE3 is stronger at 97.5 km; DW1(*U*) and DW1(*V*) peak at tropical latitudes, whereas DE3 (*U*) peaks near the equator. Further, DW1(*T*)-DW1(*V*) and DE3(*T*)-DE3(*U*) pairs have similar intraannual variability and can be used for intercomparison. There have been similar reports on the seasonal behavior of DE3 from UARS [*Forbes et al*., 2003b] and TIMED [*Oberheide and Forbes*, 2008] satellite observations.

5. Possible Solar Cycle Influence on Tides and the Background Atmosphere

Before we compare the diurnal tide from ground- and space-based observations, it is to be noted that there is an apparent long-term trend in RDm amplitudes, with enhanced diurnal tide activity observed during the solar minimum years of 2006–2009 and reduced tidal activity during the solar maximum years of 1999–2003. To extract such a signature with a period roughly the same as that of a solar cycle, we use singular spectrum analysis (see *Ghil et al*. [2002] for a useful reference). Here the estimated tidal amplitudes (RDm) at 86 km for the entire duration of 1993–2011 are decomposed into the underlying trend and long-term (of the period of several years) and short-term (of time scales less than a few years) variations. The first principal component with the longest temporal scale of variability has a period very similar to that of the solar cycle as can be seen in Figure 4 (red curve). The variable plotted therein is the first reconstructed component (RC1) which is essentially a projection of the time embedded matrix of the first principal component on its corresponding eigenvector, i.e., its empirical orthogonal function. Also shown in Figure 4 is the monthly sunspot number for the years 1993–2011 (black curve). A clear out-of-phase relation between the two is visible, especially from the year 1998 onward, indicating that there is indeed a solar cycle signature in the observed diurnal tide over Tirunelveli during this period. It can also be noticed that between 1993 and 1998 when the solar activity level decreased the tidal amplitude also decreased, which was opposite to the response seen during the later years (i.e., during 2003–2008). The correlation coefficient for the two parameters for the entire period (1993–2011) was 0.64, whereas it was 0.89 when the analysis was restricted to the period of 1998–2011.

We extend this analysis to SABER and TIDI observations as well. For this exercise, we use satellite data for the period up to October 2016. The results for the first reconstructed component for TIDI meridional wind at

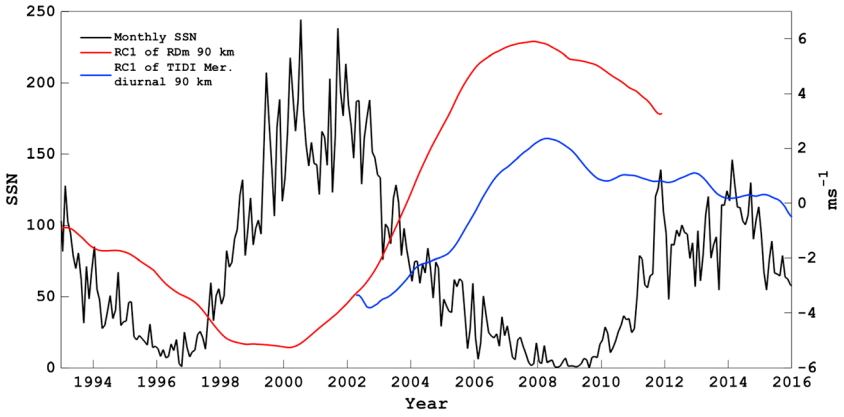

Figure 4. Comparison of the first reconstructed component of RDm at 90 km (red curve), the first reconstructed component of the diurnal tide in meridional wind at 90 km from TIDI observations (blue curve), and the monthly sunspot number for the period of 1993–2011 (black curve). See text for further details.

90 km are plotted as blue curve in Figure 4. A weak solar cycle signature is evident in the TIDI diurnal tide amplitude. Features like smaller amplitudes during the years 2002 and 2003 and larger amplitudes during 2009–2010 are consistent between the space- and ground-based observations. However, the variation in TIDI amplitude after 2008 has been subdued. When SABER data sets were examined, we could only detect a weak trend (not shown here).

For further analysis and comparison, we remove the largest scale of variability from the deduced diurnal tide amplitudes from radar observations. In Figure 5 we show RDm and the detrended values. Although both the curves agree well during 1993–1997 and 2010–2011, the differences are noticeable during the intermediate years.

We next explore whether the long-period variation seen in diurnal tidal winds can be related to any solar cycle related change in ambient densities. It may be recalled that other than temperatures, the SABER instrument has been yielding useful data on global total density fields. At thermospheric altitudes, the background densities are known to respond directly to solar activity and induce changes in thermospheric diurnal tide amplitudes [*Hedin et al.*, 1994; *Liu et al.*, 2004; *Lei et al.*, 2007; *Wu et al.*, 2012]. In the present work we used SABER densities at MLT altitudes and examined whether there were any long-term variation in densities.

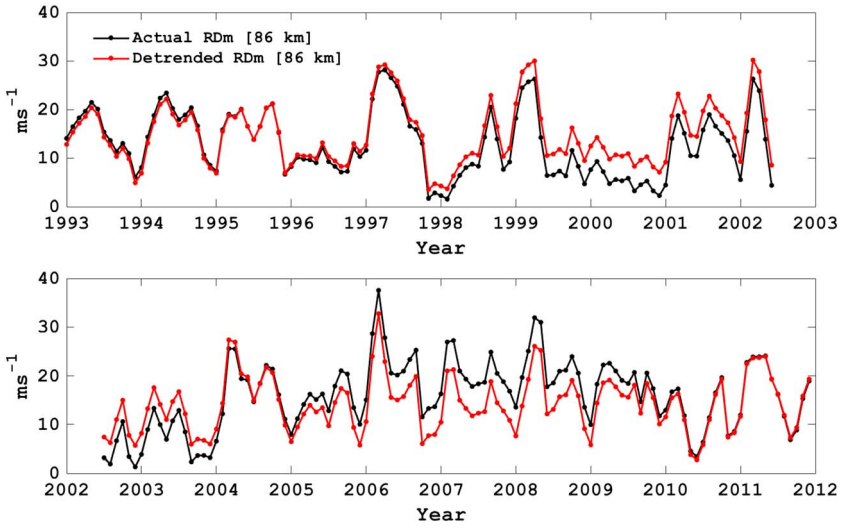

Figure 5. RDm amplitudes (black curves) along with their detrended values (red curves) (long-term variation removed) for the period of 1993–2011 (see text for details).

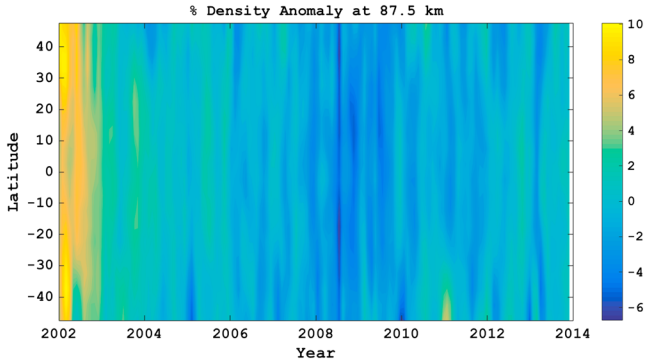

Figure 6. Latitude-month plot of the percent deviation in zonal mean densities at 87.5 km obtained from SABER for the period of 2002–2013.

The results reveal that the background neutral densities are larger during the solar maximum years of 2002–2003 and smaller during the solar minimum years of 2008–2009. Figure 6 shows the percentage change in zonal mean density from the climatological mean, and in Figure 7 we show the results for the Tirunelveli latitude, wherein we also plot the sunspot number. It is observed that the change in densities can be as large as 6–10% from climatological mean even at 87.5 km.

6. Comparison of Diurnal Amplitudes Extracted From Radar Wind, SABER Temperature, and TIDI Wind Observations

As pointed out earlier, a single ground-based station cannot resolve the zonal wave number of a tide. The diurnal tide estimated from ground-based observations is indeed a superposition of all zonal wave numbers [e.g., *Du et al*., 2007]. For comparing the results obtained from two different platforms (ground-/satellite-based), we use satellite data sets and reconstruct the tidal field for the given longitude by superposing various tidal components (zonal wave numbers) (see equations (2) to (5)). While doing so, we consider a smaller grid dimension of $\pm$2.5° in latitude centered at the latitude of Tirunelveli.

Before we present the results, a few points regarding the sampling and local time issues typically associated with such an exercise need to be mentioned. At the outset, we note that frequent gaps in hourly averaged radar data do not permit us to use them for times corresponding to TIDI overpasses. In such an exercise, several of the 60 day data segments (with all local times covered) get rejected due to insufficient number of points among the radar observations (at least 18 out of 24 hourly slots are required to be filled for the fit to be applied). Moreover, as discussed in *Hasebe et al*. [1997], *Forbes et al*. [2004], and elsewhere, the spatio-temporal scales for the two techniques are distinctly different. For these reasons, any direct comparison of tidal estimates based on "coincidence" measurements is thus less reliable.

On the other hand, it is worthwhile to assess to what extent those data collected from passes over the Tirunelveli site are "global" and to what extent they are "local." For this exercise, we performed 1-D fits (only in time domain) to those overpass data sets obtained from TIDI and compared the resultant tidal amplitudes with those reconstructed from the 2-D fits described earlier. The results for 90 km altitude are presented in Figures 8 and 9. It is remarkable that the 1-D and the 2-D fits agree quite well in both meridional and zonal components. This indicates that the TIDI overpass data, when organized in 60 day segments, can capture the global features of diurnal tide in the seasonal and interannual time scales. The greater differences in the zonal component are possibly due to the presence of smaller period oscillations with high zonal wave numbers which are not captured in the 2-D fitting scenario.

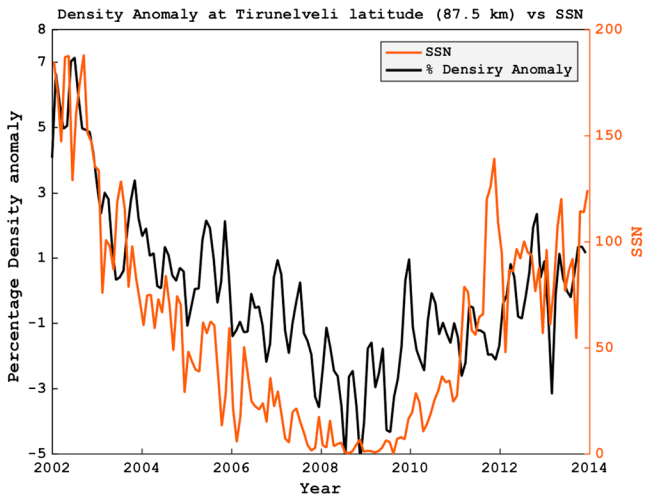

Figure 7. Percentage density anomaly (black curve) computed for Tirunelveli latitude plotted with sunspot number for the period of 2002–2013 (red curve).

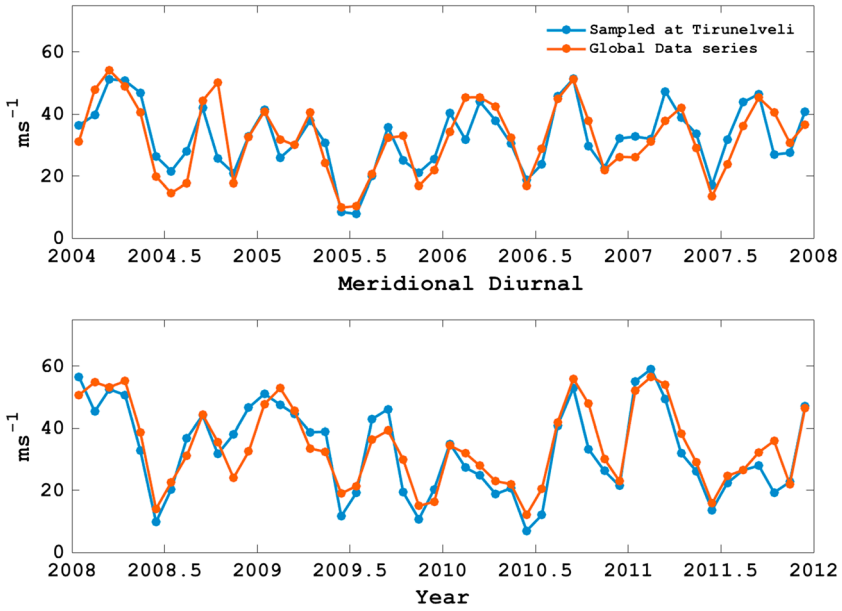

Figure 8. Comparison for TIDI diurnal tide in meridional wind obtained from the 2-D fits (red curve) versus diurnal tide estimates for meridional wind obtained from the satellite overpass data (1-D fits) (blue curve).

Keeping in mind the dominant tidal components noticed in the wave number spectra of SABER and TIDI, only DW1 is used to reconstruct the net tidal component (referred below as D(*T*)) from SABER at Tirunelveli longitudes. Figure 10 shows the comparison between RDm tide (black) and DW1 (*T*) (red) tides derived from SABER for 87.5 km. The amplitudes for both the tidal estimates are plotted in their respective units. RDm amplitudes (m s^{-1}) are shown on the ordinate scale on the left hand side, while DW1(*T*) amplitudes are shown on the ordinate scale on the right-hand side. It may be recalled that the longest temporal scale of variability in RDm has already been removed (refer to Figure 5) and so what are plotted in Figure 10 are the residuals and they are not to be treated as absolute amplitudes. It can be immediately noticed in Figure 10 that the RDm

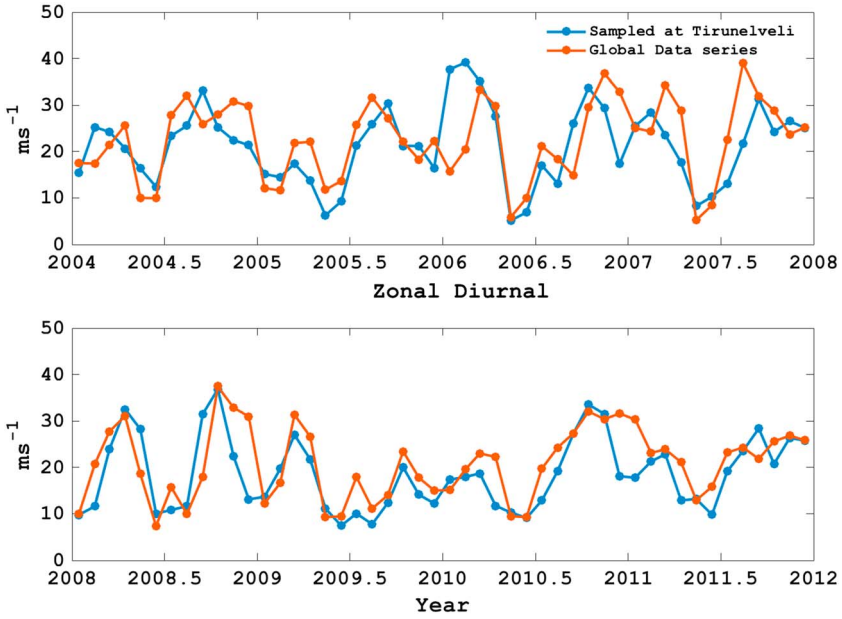

Figure 9. Same as Figure 8 but for zonal component.

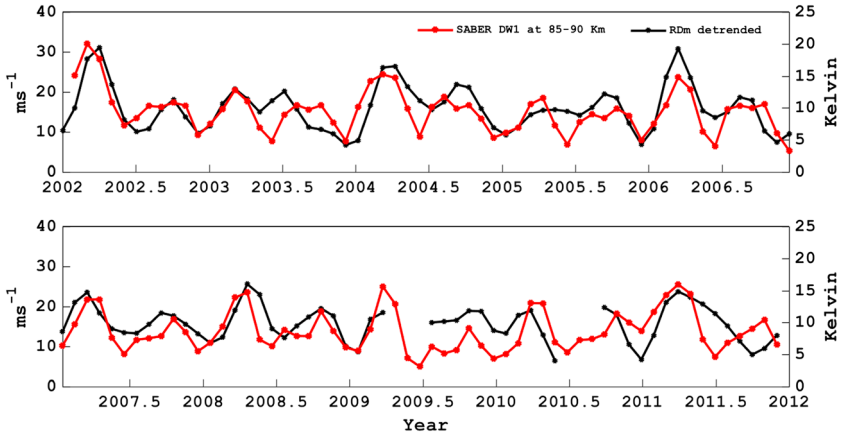

Figure 10. RDm amplitudes (black curves) compared with DW1 tide from SABER observations (red curves).

tide and the DW1(*T*) tide show a clear covariability with a correlation coefficient of ~0.7. It is important to note that the correlation coefficient only marginally improves after the inclusion of DE3. Both RDm and DW1(*T*) show consistency in terms of their SAO and QBO-like features.

Similar variations of RDm and DW1(*T*) tides in the seasonal and interannual time scales can be understood by examining the diurnal wave spectrum obtained from SABER data. Looking at the results depicted in Figure 1a, it is evident that this region is dominated by the DW1 tide, whereas DE3 starts dominating at higher altitudes. The result is important in itself as it points out that a significant portion of tides at an altitude of ~88 km observed by the ground-based radar can be attributed to DW1 tide, at least in the meridional wind component.

For comparison with TIDI, we make use of the observations corresponding to 90 km. Again, only the major tidal components are used for reconstruction of the satellite tidal wind field for the ground radar site. Figure 11 shows the comparison of RDm (black curve) with DW1(*V*) (blue curve) and D(*V*) (DW1(*V*) + DE3(*V*)) (red curve)). We would like to caution the readers that the TIDI wind amplitudes are double the radar-derived wind amplitudes. In this context, we may recall that the discrepancies in tidal amplitudes between the satellite and radar observations are known to the scientific community [e.g., *Khattatov et al.*, 1996; *Forbes et al.*, 2004]. In a recent review, the reasons for the underestimation of winds by MF/HF radar systems are well discussed [*Reid*, 2015].

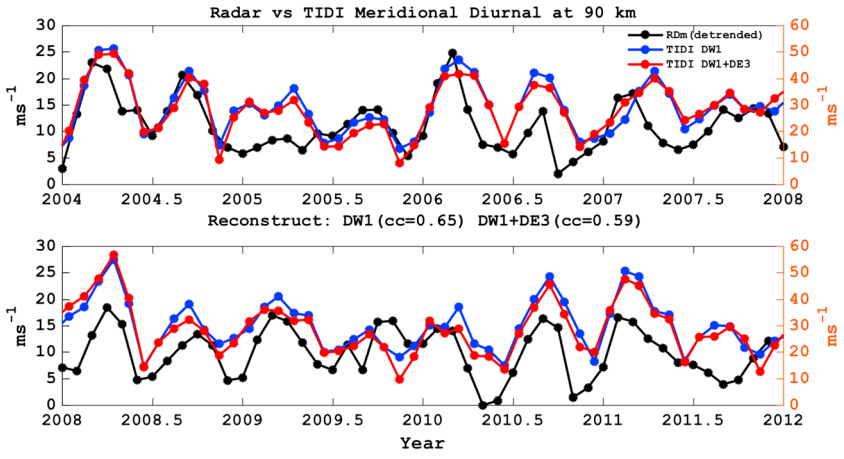

Figure 11. RDm amplitudes (black curves) compared with TIDI results (for meridional wind) (blue curves for DW1 tide alone and red curves for DW1 and DE3 tides superposed).

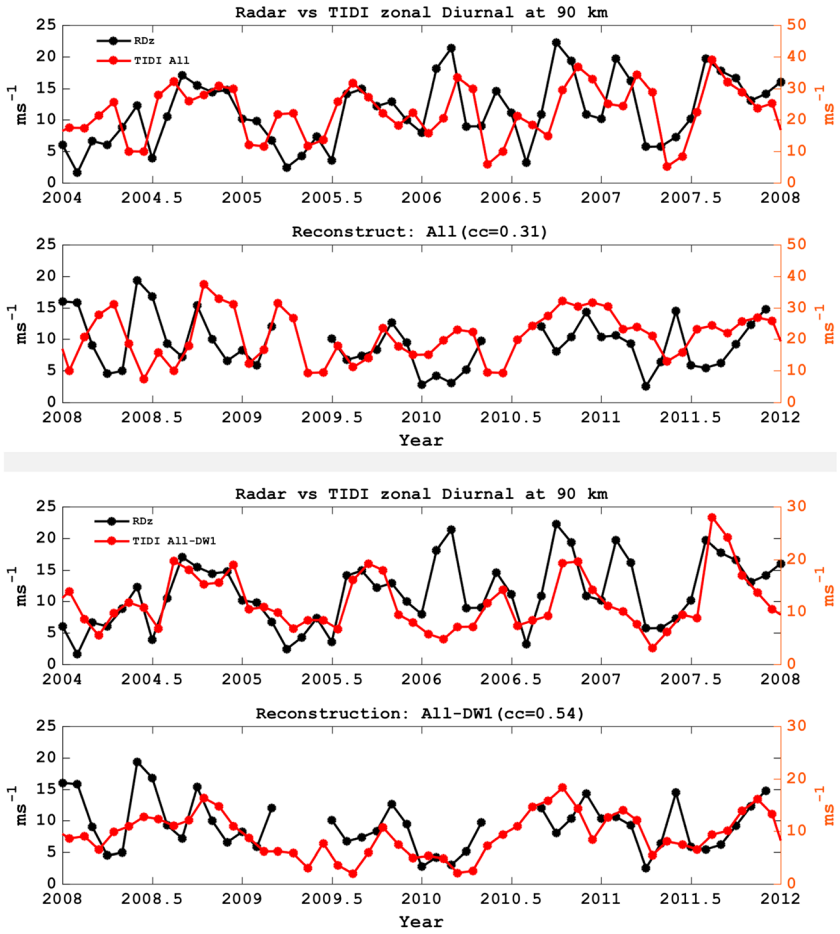

Figure 12. RDz amplitudes (black curves) compared with TIDI results (for zonal wind) (red curves) (all tidal components superposed are shown in the top two panels, and all tidal components minus DW1 are shown in the bottom two panels).

In spite of the underestimation of winds by the radar, the agreement between RDm and DW1(*V*) in terms of their variability is generally good with a correlation coefficient of 0.65. This is encouraging given the long duration (a span of eight years) over which the comparison is being made. However, the correlation is relatively smaller for TIDI and this is because of the discrepancy for the year 2005 wherein the TIDI amplitudes differed considerably from the radar estimates. Note that SABER results show smaller amplitudes during 2005.

As mentioned earlier, the zonal component is dominated by nonmigrating tides, and so we include all nonmigrating components while reconstructing the tidal field in the zonal direction for the ground site. Figure 12 shows the comparison between RDz (shown as black curves) and the reconstructed diurnal tide in zonal wind. The red curve in the top two panels represents the reconstructed tide with all components included, whereas the red curve in the bottom two panels includes all components except DW1. The discrepancies between the reconstructed and the radar observed tidal fields are reduced when DW1 is not included for reconstruction. The correlation coefficients turned out to be 0.31 and 0.54, respectively, for the two cases.

Although the reports from the CAWSES tidal campaign had suggested that both radar and satellite derived results depict the same tidal fields [*Ward et al*., 2010], considerable discrepancies are evident as reflected in the correlation analysis presented above. It is possible that local tides are stronger in the zonal component than in the meridional component, and therefore, the ground-based radars sense the signatures of local tides in the zonal wind component to a greater extent than in the meridional wind component. In their comparison study taken up with the Wind Imaging Interferometer and ground-based radar observations, *Portnyagin et al*. [1999] found systematic biases for mean zonal winds. A few other studies pointed out

that there was a tendency for the meridional component to have a better agreement with satellite observations than the zonal component [*Forbes et al*., 2004]. *Kishore Kumar et al*. [2014] noticed a smaller correlation for the diurnal tide in zonal wind than in the meridional component while comparing ground-based observations with the global-scale wave model simulations. We thus make a point here that the differences between the zonal and meridional wind comparisons with satellite observations are not new to the scientific community and the reasons for them are yet to be understood.

7. Discussion

Global-scale waves are characterized by both their temporal and spatial structures. A single ground station will be unable to delineate the underlying components, as spatial information over the global scale cannot be obtained from single-station observations. Satellite-based observations provide an optimum way out for delineating global-scale waves, but at the cost of good temporal resolution. For meaningful scientific returns from either of the experimental data, it is indeed desirable to check for any inconsistency between the two sets of observations.

There have been studies dealing with the consistency between the tidal signatures derived from ground- and satellite-based observations. The first observations from the UARS satellite revealed several discrepancies between the tidal signatures measured on ground and those sampled by space-based observations [e.g., *Khattatov et al*., 1996]. The discrepancies reported were largely due to the limitations of individual instruments and the measurement techniques adopted [*Hasebe et al*., 1997; *Forbes et al*., 2004]. Satellite observations generally have large sampling volume, and the wind fields are considered homogeneous in this volume. This averages out the effects of any small-scale waves. On the other hand, smaller sampling volumes of radars enable them to observe small-scale features like gravity waves. Further, within the MLT region, radars might be detecting ionized structures moving in response to the ambient electric field at certain heights (above 90 km, in particular), and therefore, the radars operating on this region might not be sampling the true neutral winds of interest [e.g., *Gurubaran and Rajaram*, 2000].

Earlier consistency studies did not take into account the presence of nonmigrating tides, although they were identified as a possible source of discrepancy then [*Khattatov et al*., 1996]. In a later study, *Lu et al*. [2011] examined the consistency between the diurnal tides derived from the TIMED satellite and a ground-based radar. *Huang et al*. [2006] investigated the consistency between TIDI and HRDI diurnal winds and temperatures and reported certain discrepancies between the two data sets, especially in the zonal component. A more focused study, though restricted to a limited duration, was carried out by *Ward et al*. [2010]. The study pertains to worldwide observational campaigns whose periods were restricted to 2 month duration, and therefore, this study did not take into account the seasonal variation. When additional tidal components were incorporated in the reconstruction of tidal fields at the respective ground sites, the agreement between the ground and satellite diurnal tide signatures turned out to be good.

There have been a number of other comparisons between radar and satellite data sets [e.g., *Portnyagin et al*., 1999; *Forbes et al*., 2004; *John et al*., 2011; *Killeen et al*., 2006; *Kishore Kumar et al*., 2014; *Guo and Lehmacher*, 2009], but they were all short-term studies. We would like to point out here that there exist no previous long-term consistency studies using space- and ground-based observations of diurnal tide in the MLT region. The present study is unique in the sense that it utilizes nearly a decadelong simultaneous data for long-term comparison of the data sets from low latitudes. In this work we consider both zonal and meridional wind components unlike a few other studies that used either of the two. We summarize the results below.

The seasonal variability of the diurnal tide is different in different parameters. Within the MLT region and in seasonal time scales, the migrating DW1 shows similar variability in temperature and meridional wind, whereas the nonmigrating DE3 shows similar variability in temperature and zonal wind. Also, in general, the amplitude of the DE3 signature in zonal wind is almost double than that of the meridional wind. The DE3 tide is known to be the vertical extension of the zonal wave number 3 Kelvin wave with its characteristic larger wind magnitude in the zonal direction [*Forbes et al*., 2003a]. On the other hand, DW1 signatures are stronger in the meridional wind than in the zonal wind. Both DW1 in the zonal component and DE3 in the meridional component show triannual variation. Although scattered reports are available on most of these features [e.g., *Talaat and Lieberman*, 1999; *Zhang et al*., 2006; *Oberheide et al*., 2006; *Mukhtarov et al*., 2009], the present work gathers in one place the observational findings of the seasonal and long-term

variabilities of diurnal tide in temperatures and winds in the MLT region in a concise manner. For reasons stated in the previous section, we chose to use space-time (or 2-D) least squares fitting of satellite data instead of directly using overpass data representing "coincident" measurements.

In seasonal time scales, our results reveal that the meridional diurnal winds observed by the MF radar correlate well with the DW1 tide derived from SABER (refer to Figure 10). These are consistent in long term, with both data sets revealing intraannual (SAO-like features with equinoctial maxima, for example) and interannual (QBO-like features) variability. The correlation between the two is remarkable considering that these are two different parameters measured by different techniques from different platforms. Also, radar and TIDI winds for the meridional component agree reasonably well (refer to Figure 11). The comparison for the TIDI zonal wind and RDz is not so encouraging, but the correlation improves when DW1 is removed from the 2-D fitting (refer to Figure 12). We thus infer from the above that the long-term variability of the diurnal tide in meridional wind between 85 and 90 km is primarily contributed by DW1, as nonmigrating tides are relatively less strong in this wind component at those altitudes. Whereas, the diurnal tide in zonal wind is seen to be influenced more by nonmigrating tidal features in the MLT region. It is also likely that the 2-D fitting employed for TIDI data sets is not able to capture modes of oscillation of high zonal wave number which the radar can "see."

Khattatov et al. [1996] suggested different spatial resolution of the instruments and short-term variability as the possible causes for the difference between the tidal signatures derived from the two data sets. *Ward et al*. [2010] suggested that most of the discrepancies can be addressed by superposing the migrating and nonmigrating components from the satellite observations and comparing the reconstructed tidal field with the ground observations. As we have seen in this work, there are still subtle differences in the tidal signatures, especially when long-term data sets are analyzed.

Another aspect of the results presented in this study is the highly variable nature of nonmigrating tides. Some tidal components or parts of their variability appear year after year while others do not appear over consecutive years thereby exhibiting significant interannual variability. This is an important factor to be considered in any study that addresses the vertical coupling of atmospheric regions, as this variability can be traced back to the lower and middle atmosphere.

The reason for the differing behavior of the diurnal tide in zonal and meridional winds detected in ground radar observations [e.g., *Gurubaran et al*., 2009] was not known earlier. In the present work we attribute part of these differences to how different tidal components operate on the two wind components at different times. *Gurubaran and Rajaram* [1999] also noticed an additional peak in zonal diurnal winds during the month of June. As revealed in the present work, this additional peak seems to be contributed by zonal DW1 tide, which is enhanced during these months.

In a recent study, *Riggin and Lieberman* [2013] compared zonal diurnal wind observed by an equatorial radar with migrating diurnal temperatures observed by SABER. Their study brought out the discrepancy in the vertical structure between the two. In the context of the results presented in this work, one can expect such a discrepancy as we are looking at two different tidal patterns. It should be noted that at low latitudes DW1 is dominant in the meridional wind, whereas the zonal winds are influenced more by nonmigrating tides, which could dominate the zonal component even at lower altitudes. In this context, the vertical structure of the deduced tidal features in winds may not bear any resemblance to the vertical structure of diurnal temperatures deduced from satellite observations. We therefore suggest that both vertical structure and the temporal behavior of a tide might be different in different parameters. Thus, care must be taken while comparing two different parameters in both altitude and temporal domains.

In agreement with the earlier results of *Sridharan et al*. [2010], tidal winds were shown to be stronger during the solar minimum years of 2005–2009, whereas they were weaker during the solar maximum years of 1999–2003. The diurnal tide amplitudes derived from radar observations were subjected to the singular spectrum analysis. The first principal component with its longest temporal scale of variability was identified as having a period similar to that of the solar cycle. When a similar analysis was carried out for TIDI observations, we notice a somewhat subdued signature in the diurnal tide in the meridional wind field at 90 km (refer to Figure 4). SABER data sets, however, reveal long-term variation in background parameters, namely, the zonal mean temperature and density, over the height region of 85–90 km. In particular, our analysis of SABER data sets reveals a distinct solar cycle signature in the MLT zonal mean density at these heights. The variation in

density during a solar cycle period is ~6–10% over climatological means. The change in zonal mean temperature is, however, ~4% only.

Using a variety of data sets and adopting Hough Mode Extensions, *Oberheide et al*. [2009] studied the long-term variability of DE3 tide from the MLT region to the ionosphere. Though restricted to the period of 2002–2007, their results revealed solar cycle effects on thermospheric parameters at altitudes above 120 km. Within the thermosphere, the density and winds are shown to be most sensitive, whereas the temperature tide is less affected. No perceptible solar cycle dependence could be found in the MLT region, although the authors emphasized on the need for extended data sets that would be required to correctly decipher the solar cycle signature.

Zhu et al. [2015] examined the solar cycle influence on volume emission rates of nighttime green line emission and atomic oxygen abundances over the altitude region 92–104 km using a variety of data sets. Noting that the solar cycle impact results in the increase of atomic oxygen abundance with altitude and in the increase of total densities (from 5% at 92 km to 7% at 96 km in terms of percent variation) in SABER data sets, the authors conclude that the variations in atomic oxygen abundances are probably driven by the total density variations induced by atmospheric compression and expansion during the solar cycle.

Turning our attention toward the results presented in this work, the total density changes in SABER over the period of the solar cycle (2002–2013) are real and going by the interpretation of *Zhu et al*. [2015], it is opined that the atmospheric "breathing-in" and "breathing-out" process results in compressive and expansive effects in the mesopause region leading to density enhancement and reduction as the solar cycle progresses. As tides in the mesopause region are subject to damping by eddy diffusion, the ambient density changes can have an indirect control on the variability of diurnal tide over the corresponding time scales. Model simulations like those incorporating a suitable parameterization scheme for the eddy diffusion operating on longer time scales are the need of the hour, and this would throw some light into the mechanisms responsible for the variability of the diurnal tide over the solar cycle time period.

8. Conclusion

An important goal of the present work is to examine the consistency in the diurnal tide in the MLT region as observed by ground-based radars and satellite-based instruments. As reported herein, DW1 is the dominant tidal mode in SABER temperatures and in the meridional wind observed by both MF radar and TIDI and is consistent in all three data sets. On the other hand, notable differences exist in the tidal fields retrieved from the TIDI zonal wind/SABER temperature observations and radar zonal wind measurements. Other than nonmigrating tides, nontidal or local influences seem to play an important role in determining the variability of the diurnal tide in zonal wind observed by ground-based radars in all time scales.

Another feature reported in this work is the solar cycle influence of the diurnal tide as observed by the radar at Tirunelveli, a feature not so prominently seen in the tidal amplitudes estimated from SABER temperature and TIDI wind data sets. In this work, we notice a solar cycle variation evident in zonal mean ambient densities at heights as low as 87.5 km in SABER observations. It is suggested that density changes caused by the atmospheric expansion and compression induce changes in eddy diffusion giving rise to corresponding variation in diurnal tide. There was one exception noticed while comparing the radar tidal amplitudes and the monthly sunspot number. During the years 1993–1996 when the sunspot number decreased, the tidal amplitudes also decreased indicating that the response of the diurnal tide to the solar cycle variation was poorer during this period. This could imply that there are other agencies which might have taken part in influencing the long-term diurnal tide variability.

Model simulations with a suitable parameterization scheme incorporating the effects of damping on the diurnal tide can throw some lights on the solar cycle influence on tides reported in this work. There is also a need to consider any long-term variations of phenomena like QBO and El Niño–Southern Oscillation that could modify the scenario of a simple linear response of the tides to solar variability.

Acknowledgments
The authors gratefully acknowledge the contributions of SABER and TIDI teams of TIMED mission in providing useful scientific data for the studies pursued herein. SABER Version 2 data can be downloaded from http://saber.gats-inc.com/data_v2.php. TIDI level 3 vector winds can be accessed at ftp://tidi.engin.umich.edu/tidi/vector/. One of the authors (D.S.) thanks the director, Indian Institute of Geomagnetism, for a research scholarship. The MF radar at Tirunelveli is operated by the Indian Institute of Geomagnetism, and the authors are grateful to the excellent technical support provided by K. Unnikrishnan Nair and his colleagues in running the radar system since 1992. Any request for the Tirunelveli MF radar data for the period under the present study may be sent to S.G. This work is supported by the Department of Science and Technology, Government of India.

References

Chang, L. C., et al. (2012), Comparison of diurnal tide in models and ground-based observations during the 2005 equinox CAWSES tidal campaign, *J. Atmos. Sol. Terr. Phys.*, *78–79*, 19–30.

Du, J., W. E. Ward, J. Oberheide, T. Nakamura, and T. Tsuda (2007), Semidiurnal tides from the extended Canadian Middle Middle Atmosphere Model (CMAM) and comparisons with TIMED Doppler Interferometer (TIDI) and meteor radar observations, *J. Atmos. Sol. Terr. Phys.*, *69*, 2159–2202.

Forbes, J. M. (1995), Tidal and planetary waves, in *The Upper Mesosphere and Lower Thermosphere: A Review of Experiment and Theory*, edited by R. M. Johnson and T. L. Killeen, AGU, Washington, D. C., doi:10.1029/GM087p0067.

Forbes, J. M., M. E. Hagan, S. Miyahara, Y. Miyoshi, and X. Zhang (2003a), Diurnal nonmigrating tides in the tropical lower thermosphere, *Earth Planets Space*, *55*, 419–426.

Forbes, J. M., X. Zhang, E. R. Talaat, and W. Ward (2003b), Nonmigrating diurnal tides in the thermosphere, *J. Geophys. Res.*, *108*(A1), 1033, doi:10.1029/2002/JA009262.

Forbes, J. M., Y. I. Portnyagin, W. Skinner, R. A. Vincent, T. Solovjova, E. Merzlyakov, T. Nakamura, and S. Palo (2004), Climatological lower thermosphere winds as seen by ground-based and space-based instruments, *Ann. Geophys.*, *22*, 1931–1945.

Forbes, J. M., X. Zhang, S. Palo, J. Russell, C. J. Mertens, and M. Mlynczak (2008), Tidal variability in the ionospheric dynamo region, *J. Geophys. Res.*, *113*, A02310, doi:10.1029/2007JA012737.

Gan, Q., J. Du, W. E. Ward, S. R. Beagley, V. I. Fomichev, and S. Zhang (2014), Climatology of the diurnal tides from eCMAM30 (1979 to 2010) and its comparison with SABER, *Earth Planets Space*, *66*, 103, doi:10.1186/1880-5981-66-103.

Garcia- Comas, M., et al. (2008), Errors in Sounding of the Atmosphere using Broadband Emission Radiometry (SABER) kinetic temperature caused by non-local-thermodynamic-equilibrium model parameters, *J. Geophys. Res.*, *113*, D24106, doi:10.1029/2008JD010105.

Ghil, M., et al. (2002), Advanced spectral methods for climatic time series, *Rev. Geophys.*, *40*(1), 1003, doi:10.1029/2000RG000092.

Guo, L., and G. Lehmacher (2009), First meteor radar observations of tidal oscillations over Jicamarca (11.95° S, 76.87° W), *Ann. Geophys.*, *27*, 2575–2583, doi:10.5194/angeo-27-2575-2009.

Gurubaran, S., and R. Rajaram (1999), Long-term variability in the mesospheric tidal winds observed by MF radar over Tirunelveli (8.7°N, 77.8°E), *Geophys. Res. Lett.*, *26*, 1113–1116, doi:10.1029/1999GL900171.

Gurubaran, S., and R. Rajaram (2000), Signatures of equatorial electrojet in the mesospheric partial reflection drifts over magnetic equator, *Geophys. Res. Lett.*, *27*, 943–946, doi:10.1029/1999GL003733.

Gurubaran, S., R. Rajaram, T. Nakamura, T. Tsuda, D. Riggin, and R. A. Vincent (2009), Radar observations of the diurnal tide in the tropical mesosphere-lower thermosphere region: Longitudinal variabilities, *Earth Planets Space*, *61*, 513–524, doi:10.1186/BF03353168.

Hagan, M. E., and J. M. Forbes (2002), Migrating and nonmigrating diurnal tides in the middle and upper atmosphere excited by tropospheric latent heat release, *J. Geophys. Res.*, *107*(D24), 4754, doi:10.1029/2001JD001236.

Hagan, M. E., and J. M. Forbes (2003), Migrating and non-migrating semidiurnal tides in the upper atmosphere excited by tropospheric latent heat release, *J. Geophys. Res.*, *108*(A2), 1062, doi:10.1029/2002JA009466.

Hagan, M. E., and R. G. Roble (2001), Modeling diurnal tidal variability with the National Center for Atmospheric Research thermosphere-ionosphere-mesosphere-electrodynamics general circulation model, *J. Geophys. Res.*, *106*, 24,869–24,882, doi:10.1029/2001JA000057.

Hasebe, F., T. Tsuda, T. Nakamura, and M. D. Burrage (1997), Validation of HRDI MLT winds with meteor radars, *Ann. Geophys.*, *15*, 1142–1157, doi:10.1007/s00585-997-1142-7.

Hedin, A. E., M. J. Buonsanto, M. Codrescu, M. L. Duboin, C. G. Fesen, M. E. Hagan, and D. P. Sipler (1994), Solar activity variations in midlatitude thermospheric meridional winds, *J. Geophys. Res.*, *99*, 17,601–17,608, doi:10.1029/94JA01134.

Huang, F. T., H. G. Mayr, C. A. Reber, T. Killeen, J. Russell, M. Mlynczak, W. Skinner, and J. Mengel (2006), Diurnal variations of temperature and winds inferred from TIMED and UARS measurements, *J. Geophys. Res.*, *111*, A10S04, doi:10.1029/2005JA011426.

John, S. R., K. Kishore Kumar, K. V. Subrahmanyam, G. Manju, and Q. Wu (2011), Meteor radar measurements of MLT winds near the equatorial electro jet region over Thumba (8.5°N, 77°E): comparison with TIDI observations, *Ann. Geophys.*, *29*, 1209–1214, doi:10.5194/angeo-29-1209-2011.

Khattatov, B. V., et al. (1996), Dynamics of the mesosphere and lower thermosphere as seen by MF radars and by the high-resolution Doppler imager/UARS, *J. Geophys. Res.*, *101*, 10,393–10,404, doi:10.1029/95JD01704.

Killeen, T. L., Q. Wu, S. C. Solomon, D. A. Ortland, W. R. Skinner, R. J. Niciejewski, and D. A. Gell (2006), TIMED Doppler Interferometer: Overview and recent results, *J. Geophys. Res.*, *111*, A10S01, doi:10.1029/2005JA011484.

Kishore Kumar, G., W. Singer, J. Oberheide, N. Grieger, P. P. Batista, D. M. Riggin, H. Schmidt, and B. R. Clemesha (2014), Diurnal tides at low latitudes: Radar, satellite, and model results, *J. Atmos. Sol. Terr. Phys.*, *118*, 96–105, doi:10.1016/j.jastp.2013.07.005.

Lei, J., R. G. Roble, S. Kawamura, and S. Fukao (2007), A simulation study of thermospheric neutral winds over the MU radar, *J. Geophys. Res.*, *112*, A04303, doi:10.1029/2006JA012038.

Liu, L., X. Luan, W. Wan, J. Lei, and B. Ning (2004). Solar activity variations of equivalent winds derived from global ionosonde data. *J. Geophys. Res.*, *109*, A12305, doi:10.1029/2004JA010574.

Lu, X., A. Z. Liu, J. Oberheide, Q. Wu, T. Li, Z. Li, G. R. Swenson, and S. J. Franke (2011), Seasonal variability of the diurnal tide in the mesosphere and lower thermosphere over Maui, Hawaii (20.7°N, 156.3°W), *J. Geophys. Res.*, *116*, D17103, doi:10.1029/2011JD015599.

Mayr, H. G., J. G. Mengel, E. R. Talaat, H. S. Porter, and K. L. Chan (2005), Mesospheric non-migrating tides generated with planetary waves: I. Characteristics, *J. Atmos. Sol. Terr. Phys.*, *67*, 959–980, doi:10.1016/j.jastp.2005.03.002.

Mukhtarov, P., D. Pancheva, and B. Andonov (2009), Global structure and seasonal and interannual variability of the migrating diurnal tide seen in the SABER/TIMED temperatures between 20 and 120 km, *J. Geophys. Res.*, *114*, A02309, doi:10.1029/2008JA013759.

Oberheide, J., and J. M. Forbes (2008), Tidal propagation of deep tropical cloud signatures into the thermosphere from TIMED observations, *Geophys. Res. Lett.*, *35*, L04816, doi:10.1029/2007GL032397.

Oberheide, J., Q. Wu, T. L. Killeen, M. E. Hagan, and R. G. Roble (2006), Diurnal nonmigrating tides from TIMED Doppler Interferometer wind data: Monthly climatologies and seasonal variations, *J. Geophys. Res.*, *111*, A10S03, doi:10.1029/2005JA011491.

Oberheide, J., J. M. Forbes, K. Häusler, Q. Wu, and S. L. Bruinsma (2009), Tropospheric tides from 80 to 400 km: Propagation, interannual variability, and solar cycle effects, *J. Geophys. Res.*, *114*, D00I05, doi:10.1029/2009JD012388.

Pancheva, D., and P. Mukhtarov (2011), Atmospheric tides and planetary waves: Recent progress based on SABER/TIMED temperature measurements (2002–2007), in *Aeronomy of the Earth's Atmosphere and Ionosphere*, pp. 19–56, Springer, Netherlands.

Portnyagin, Y. I., T. V. Solovjova, and D. Y. Wang (1999), Some results of comparison between the lower thermosphere zonal winds as seen by the ground-based radars and WINDII on UARS, *Earth Planets Space*, *51*(7–8), 701–709.

Rajaram, R., and S. Gurubaran (1998), Seasonal variabilities of low-latitude mesospheric winds, *Ann. Geophys.*, *16*, 197–204, doi:10.1007/s00585-998-0197-4.

Reid, I. M. (2015), MF and HF radar techniques for investigating the dynamics and structure of the 50 to 110 km height region: A review, *Progr. Earth Planet. Sci.*, *2*, 33, doi:10.1186/s40645-015-0060-7.

Riggin, D. M., and R. S. Lieberman (2013), Variability of the diurnal tide in the equatorial MLT, *J. Atmos. Sol. Terr. Phys.*, *102*, 198–206, doi:10.1016/j.jastp.2013.05.011.

Sakazaki, T., M. Fujiwara, X. Zhang, M. E. Hagan, and J. M. Forbes (2012), Diurnal tides from the troposphere to the lower mesosphere as deduced from TIMED/SABER satellite data and six global reanalysis data sets, *J. Geophys. Res.*, *117*, D13108, doi:10.1029/2011JD017117.

Skinner, W. R., et al. (2003), Operational performance of the TIMED Doppler Interferometer (TIDI), *Proc. SPIE*, *5157*, 47–57.

Sridharan, S., T. Tsuda, and S. Gurubaran (2010), Long-term tendencies in the mesosphere/lower thermosphere mean winds and tides as observed by medium frequency radar at Tirunelveli (8.7°N, 77.8°E), *J. Geophys. Res.*, *115*, D08109, doi:10.1029/2008JD011609.

Svoboda, A. A., J. M. Forbes, and S. Miyahara (2005), A space-based climatology of diurnal MLT tidal winds, temperatures and densities from UARS wind measurements, *J. Atmos. Sol. Terr. Phys.*, *67*, 1533–1543, doi:10.1016/j.jastp.2005.08.018.

Talaat, E. R., and R. S. Lieberman (1999), Nonmigrating diurnal tides in mesospheric and lower-thermospheric winds and temperatures, *J. Atmos. Sci.*, *56*, 4073–4087.

Truskowski, A. O., J. M. Forbes, X. Zhang, and S. E. Palo (2014), New perspectives on thermosphere tides: 1. Lower thermosphere spectra and seasonal-latitudinal structures, *Earth Planets Space*, *66*, 136, doi:10.1186/s40623-014-0136-4.

Ward, W. E., et al. (2010), On the consistency of model, ground-based, and satellite observations of tidal signatures: Initial results from the CAWSES tidal campaigns, *J. Geophys. Res.*, *115*(D7), D07107, doi:10.1029/2009JD012593.

Wu, Q., D. A. Ortland, B. Foster, and R. G. Roble (2012), Simulation of nonmigrating tide influences on the thermosphere and ionosphere with a TIMED data driven TIEGCM, *J. Atmos. Sol. Terr. Phys.*, *90*, 61–67.

Zhang, X., J. M. Forbes, M. E. Hagan, J. M. Russell III, S. E. Palo, C. J. Mertens, and M. G. Mlynczak (2006), Monthly tidal temperatures 20–120 km from TIMED/SABER, *J. Geophys. Res.*, *111*, A10S08, doi:10.1029/2005JA011504.

Zhu, Y., M. Kaufmann, M. Ern, and M. Riese (2015), Nighttime atomic oxygen in the mesopause region retrieved from SCIAMACHY O(^{1}S) green line measurements and its response to solar cycle variation, *J. Geophys. Res. Space Physics*, *120*, 9057–9073, doi:10.1002/2015JA021405.